Detecting Tourette's Syndrome in Anatomical Regions of the Brain through MRI Analysis and Naive Bayes Classifier

Murilo Costa De Barros[1][a], Kaue Tartarotti Nepomuceno Duarte[2][b], Wang-Tso Lee[3][c],
Chia-Jui Hsu[4] and Marco Antonio Garcia De Carvalho[1][d]

[1]*Computing Visual Laboratory, School of Technology UNICAMP, R. Paschoal Marmo, 1888,*
Jd. Nova Itália, 13484-332, Limeira, São Paulo, Brazil
[2]*Vascular Imaging Laboratory, Calgary University, 2500 University Dr. NW, Calgary, AB T2N 1N4, Canada*
[3]*Department of Pediatrics, National Taiwan University Children's Hospital, Taipei, Taiwan*
[4]*Department of Pediatrics, National Taiwan University Hospital Hsinchu Branch, Taipei, Taiwan*

Keywords: Classification, Tourette Syndrome, GLCM, Naive Bayes, Image Processing, Segmentation.

Abstract: Tourette Syndrome (TS) is an inherited condition represented by involuntary vocal and motor movements (tics). Nowadays, there is no available cure, only psychological treatments to inhibit it, requesting the use of medication in rare cases. The importance of diagnosing Tourette's in childhood enables a range of possible treatments that would decrease the intensity of TS, and in some cases, even stop it. In most cases, the TS diagnosis considers only clinical assessment. Analyzing the brain and its anatomical regions via imaging data can provide relevant information in order to assist doctors. This work aims to propose an approach in order to identify the most affected anatomical region of the brain by TS. The approach consists of three major steps: (i) the brain is segmented in its anatomical regions; (ii) texture patterns are extracted via Gray-level Co-occurrence Matrix for each region; finally, (iii) each brain region is evaluated using Naive Bayes classifier, determining the presence or absence of TS. We use MRI images from 68 subjects around nine years old equally divided whether has TS or not. The regions from the limbic system were relevant in the diagnosis: right-side accumbens reached 68% of accuracy; posterior and central parts of corpus callosum ranked in the top four positions. Combining the top five most predictive regions led our approach to reach 78% of accuracy. The results were significant in detecting the most affected regions in TS and providing a reliable approach to classify the brain regions accordingly.

1 INTRODUCTION

Tourette's Syndrome (TS) is a genetic-pathologic disorder that comprises neurophysiological and neuroanatomical aspects in subjects, commonly developed in between two and eighteen years old, the majority in male subjects (Hounie, 2006).

TS is characterized by uncontrolled movement disorders (motor or vocals *tics*); the most common tics are frequently blinking, shaking shoulders, and other involuntary movements. Repeated vocalization urges may be developed, such as coughing, grunting, whistling, and easing the throat These tics can often

---

[a] https://orcid.org/0000-0003-2452-8128
[b] https://orcid.org/0000-0002-4074-3672
[c] https://orcid.org/0000-0003-3231-9764
[d] https://orcid.org/0000-0002-6303-5564

be temporarily suppressed by patients who have TS, becoming overwhelming after some time. Figure 1 illustrates the most common uncontrolled facial movements caused by TS. The most complex and rare tics are related to subjects who have TS; three of them often serves as guidelines to diagnose TS:(1) coprolalia: Vocal tics with obscene and offensive words; (2) copropraxia: Motor tics with an obscene or offensive gesture; (3) echolalia: Vocal tics using words repetition or word sounds (Teixeira et al., 2011).

Kobierska (Kobierska et al., 2014) stated that coprophenomena, *i.e.*, actions of coprolalia and copropraxia, is developed in the peak period of TS where the tics start becoming more aggressive between 8 and 12-year-old phase, often in people with mental disorders and who have behavioral problems.

TS patients may present obsessive thoughts when they see a picture, a person, or any uncomfortable
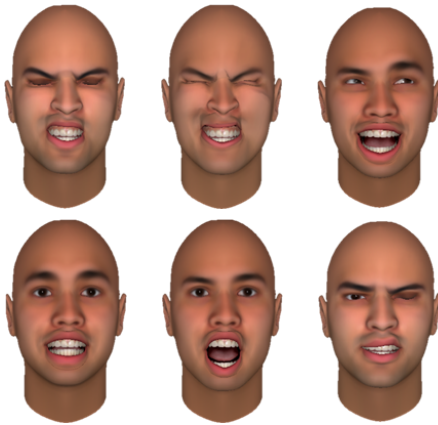
Figure 1: Common uncontrolled facial movements in a subject affected by TS.

moment that triggers high levels of anxiety and compulsive behaviors, *i.e.*, repetitive actions aiming to relieve the stress caused by those obsessions. Besides, subjects who have TS may present other disorders (Hounie, 2006) such as *Obsessive-Compulsive Disorder* (OCD) and Attention *Deficit Hyperactivity Disorder* (ADHD), posing a challenge to diagnose TS independently (Figure 2).
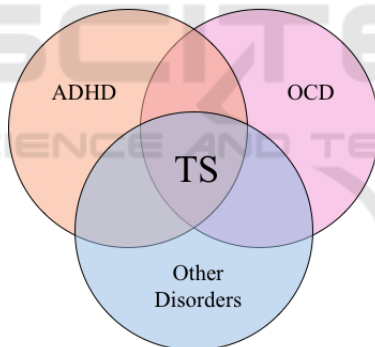

Figure 2: Disorders Intersection and TS diagnosis. Source: Adapted from (Hounie, 2006).

Medical imaging, most specifically Magnetic Resonance Imaging (MRI), plays a vital role in identifying TS and has commonly been used in the medical field to support doctors in their diagnosis (Muller, 2009). However, subtle and imperceptive changes may occur in distinct anatomical brain regions, precluding TS identification without clinical assessment. The yearning for computational approaches to automatically diagnose anatomical variation in subjects with TS using medical imaging drives the main challenge of our work.

Nowadays, *Artificial intelligence* (AI) has been adopted in different fields to improve their methods to achieve better outcomes. Not differently, the gap

between AI and the medical field has been narrowing across the years, and it has been vastly used in diseases such as Alzheimer's and Parkinson's. However, to the best of our knowledge, combining AI for anatomical brain analysis using medical imaging in TS is a novelty topic. The main contributions and features of this work are: (1) computational approach focused on TS; (2) feature-based information about brain regions for TS; (3) application of machine learning to identify the most predictive regions; (4) ensemble of the most predictive brain regions for TS. The main goal of this work is to propose an approach to automatically identify the most affected regions of TS via texture feature extraction and Naive Bayes, employing only structural MRI.

The remainder of this paper is organized as follows: Section 2 shows the related work and the gaps in the literature; the proposed approach is described in Section 3; Section 4 details the results and the list of regions affected by TS; finally, Section 5 presents the summary and conclusions.

2 RELATED WORK

Medical imaging is crucial for TS diagnosis, in addition to clinical assessments, image processing, and machine learning, and plays a vital role in interpreting brain information, thus allowing the prediction of possible outcomes for the subjects.

Muellner (Muellner et al., 2015) proposed an approach aiming to analyze the depth, opening, length and thickness of the gray matter groove in exams Diffusion Tensor Imaging (DTI). The author labeled the areas using the BrainVisa Software, improving the most affected regions, like the frontal, parietal and temporal lobes. They considered 104 subjects, half for TS and half for normal controls. In addition, adult subjects were considered instead of children, which differs from the most common approaches in the literature.

Peterson (Peterson et al., 2007) proposed an approach to analyzing the morphology of the amygdala and the hippocampus in MR scans via ANALYZE 7.5 software. The authors focused on identifying the similarity of those regions among TS subjects via Euclidean distance. For that, the images were registered to belong to the exact spatial location. They identified a smaller amygdala in children with TS.

In Tinaz (Tinaz et al., 2015), an approach was proposed to measure brain changes when patients pause their medication and treatments. Their dataset comprises 26 functional MRIs, where 13 TS subjects are aged between 18 to 46 years, and 13 normal control

subjects aged between 22 to 56 years. They reported that once the treatment had stopped, alterations in the frontal regions were shown, also reducing the right stratothalamic nodules.

The eagerness for works that employ machine learning or feature extraction for TS remains in the literature since only a few bring a computational analysis for this syndrome. However, this type of analysis has been broadly applied in diseases such as Alzheimer's and Parkinson's. Long (Long et al., 2017) analyzed the morphological changes for Alzheimer's disease and its mild cognitive impairment stages using MRI in healthy older people. The 3D T1-weighted images were segmented via FreeSurfer. The images were registered using FSL flirt to align the brain across the subjects. Next, the *Support Vector Machine* (SVM) was adopted for classification. The findings showed 96.5% accuracy in the gray matter detection, 91.74% in progressive *Mild Cognitive Impairment* (MCI), and 88.99% in the amygdala and hippocampus detection for stable MCI.

Jafarpour (Jafarpour et al., 2012) proposes a robust method to analyze MRI via feature extraction and classification. The authors address 120 MRI scans, 41 for normal control subjects and 79 for comorbidities. The authors employed a *Gray-Level Co-occurrence Matrix* (GLCM) to extract texture features, considering only a single direction $\theta = 0$ and distance $d = 1$. Finally, the descriptor outcome was clustered. They reported an accuracy higher than 92% using classifiers.

Solana-Lavalle (Solana-Lavalle and Rosas-Romero, 2021) developed an approach to predict Parkinson's disease in MRI scans. Firstly, the brain regions are segmented, and they are registered and aligned across distinct subjects. A *t* map corresponding to the difference between the labeled voxels and the region of interest is created. They reported significant results, with 99.01% of accuracy in men and 96.97% accuracy in women.

In essence, our work differs from the literature by the following topics: (1) We provide a brain segmentation via Freesurfer and feature extraction for TS subjects; (2) We propose feature-based classification using Naive Bayes for TS subjects; (3) We propose computational TS region analysis according to texture information; (4) We analyze defining the most critical regions to detect TS automatically in childhood; (5) We separated an ensemble of the best predictive regions for TS.

3 PROPOSED APPROACH

This section presents our proposed approach to address the problem of detecting TS in brain anatomical regions. Figure 3 illustrates the main steps of the proposed method: (1) image acquisition; (2) volume segmentation; (3) feature extraction; and (4) classification and majority voting. These steps will be explained in the following subsections.

1. *Image Acquisition.* including the definition of the acquisition protocol;
2. *Volume Segmentation.* using Freesurfer segmentation, dividing into distinct region groups;
3. *Feature Extraction.* applying GLCM per region volume and extracting texture information;
4. *Classification and Majority Voting.* detecting the most affected regions by TS.

3.1 Image Acquisition

The image dataset was obtained by National Taiwan University and comprises sixty-eight subjects, where thirty-four subjects have TS, and thirty-four are normal control subjects. The age is between 6 to 14 years. Table 1 summarizes the demographic information for the selected subjects.

The image dataset was acquired using a TrioTim series of the SIEMENS scanner. The MRI acquisition protocol defined 3T T1-weighted sMRI with 3mm voxel size and 192x256 matrix size. *Repetition time* (TR) equals 2000.0 and *echo time* (TE) equals 26.0. Each subject's brain volume is composed of 208 slices, enabling the construction of the entire volume to the next step.

3.2 Volume Segmentation

FreeSurfer tool was employed to segment the brain into deep-inner gray-matter regions (Fischl et al., 2002). This process mainly consists of three major steps: (1) image normalization (Figure 4 (a)) followed by skull stripping (Figure 4 (b)); (2) smoothing followed by an inflation of the surface; and (3)

Table 1: Demographic information of the selected subjects.

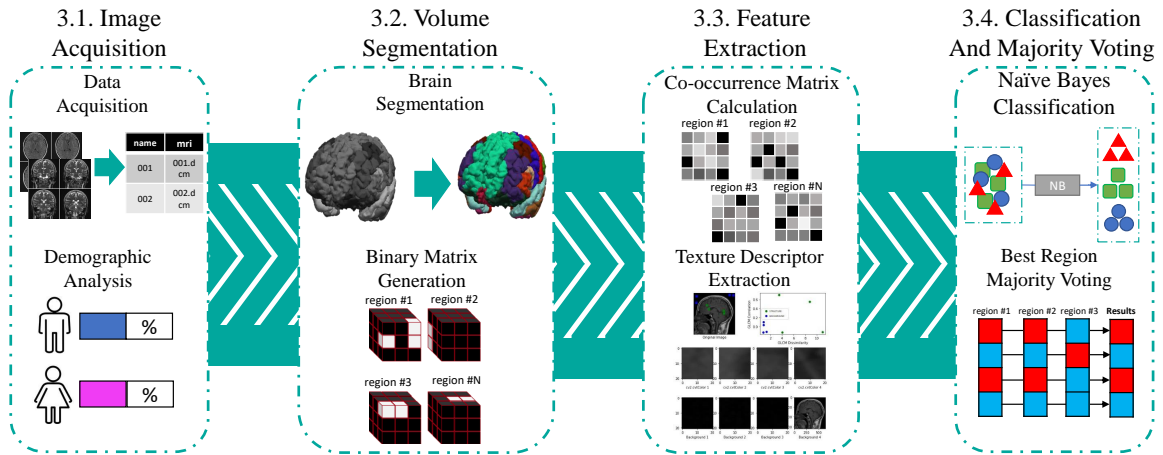| Attributes	NC (N=34)	TS (N=34)
Age (years) median (range)	6 to 14 8,94	6 to 13 8,58
Gender % male	71%	68%

Figure 3: Proposed workflow.

registration and cortical parcellation. Among the existing atlases in Freesurfer, we adopted the *Desikan-Killiany-Tourville* (DKT) atlas (Figura 4.c). We restricted the Freesurfer outcome to 30 internal gray-matter regions.

After the segmentation process, each anatomical region is represented by an unique region ID, thus allowing further comparisons across distinct subjects. Each region is separated into a three-dimensional binary volume, where the voxels are assigned to "True" when they belong to the assigned region and "False" otherwise. Thus, each subject has a set of thirty binary volumes. Figure 4 illustrates the DKT atlas segmentation applied to a particular brain volume.
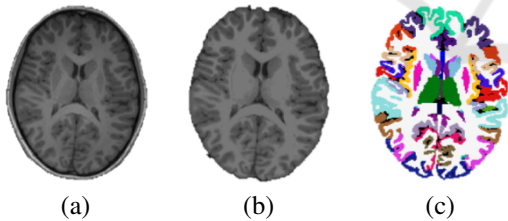

Figure 4: Pre-processing using FreeSurfer: (a) Original image normalized; (b) Skull stripping; (c) DKT-atlas.

3.3 Feature Extraction

This step is concerned to extract reliable texture features using GLCM studied by (Haralick et al., 1973) and also using radiomics according to (van Griethuysen et al., 2017). The GLCM stores the pixel/voxel affinity between a voxel value v_1 to v_2 (Figure 5). The resultant matrix is $N \times N$, where N corresponds to the maximum voxel value among the values in an image (Figure 6).

The grayscale value represents the indexes in the rows and columns, and the interaction $f(v_1, v_2)$ is the number of occurrences from v_1 towards v_2.
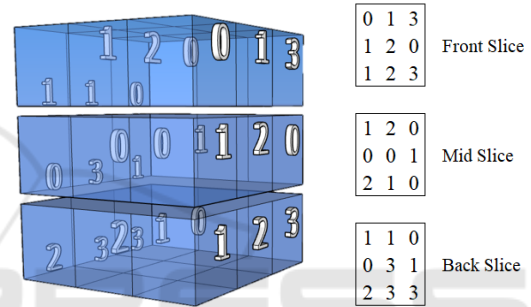

Figure 5: 3D volume where each cube corresponds to a gray-tone intensity voxel.

$$
\begin{array}{cccc}
1 & 2 & 0 & 1 \\
2 & 1 & 3 & 1 \\
2 & 1 & 0 & 2 \\
0 & 1 & 0 & 1
\end{array}
$$

Figure 6: Matrix Co-occurrence.

The transitions are calculated majorly according to two parameters: (1) θ angle (0°, 45°, 90°, 145°); and 2) distance $d = 1$. Angle corresponds to the orientation from v_1 and v_2 stored in the GLCM. Distance is defined as the interval in pixels or voxels between v_1 and v_2.

Two adaptations were adopted to GLCM: (1) since there are 3D structures (26-connectivity) instead of 2D (8-connectivity), we add more directions to calculate the displacement vector (dx, dy, dz); (2) we reformulated to rely on anatomical regions instead of the brain, disregarding occurrences of voxels that do not belong to a given region. In general, each anatomical region has a distinct GLCM.

In the end, to compose the final vector containing the information of each region per subject, twenty-three metrics to GLCM-based texture descriptors were extracted:

Autocorrelation; Joint Average; Cluster Prominence; Cluster Shade; Cluster Tendency; Contrast; Correlation; Difference Average; Difference Entropy; Difference Variance; Joint Energy; Joint Entropy; Informational Measure of Correlation 1 and 2; Inverse Difference Moment; Maximal Correlation Coefficient; Inverse Difference Moment Normalized; Inverse Difference; Inverse Difference Normalized; Inverse Variance; Maximum Probability; Sum Average; Sum Entropy; Sum of Squares (pyradiomics community, 2016)

3.4 Classification and Majority Voting

Classification. *Naive Bayes* (NB) is a probabilistic classifier based on the Bayes theorem (Zhang and Gao, 2011), part of the supervised learning branch of machine learning algorithms. This classifier independently analyzes attributes to identify its affinity to a given class. Considering a data vector $x = (x_1, x_2, x_3...x_n)$ and a set of class $w = (w_1, w_2, w_3...w_n)$, thus the probability of each class belong to a vector is represented by the expression of $p(w_i|x)$. Equation 1 states the calculation of NB (Pedrini and Schwartz, 2008).

$$P(w_i|X) = \frac{P(X|w_i) \cdot P(w_i)}{P(X)}. \quad (1)$$

where $P(w_i|X)$ is the posterior probability; $P(w_i)$ represents a given original class probability, $P(X|w_i)$ corresponds to how likely a vector x is with the class w_i. Therefore, this classification has as its decision factor two probabilities, being represented below Eq. 2.

$$P(w_i|X) > P(w_j|X). \quad (2)$$

Where $j = (1, 2, 3...n)$ with $i \neq j$

The version we applied uses the Gaussian parameter (Equation 3).

$$P(x_i|y) = \frac{1}{\sqrt{2\pi\sigma_y^2}} exp\left(-\frac{(x_i - \mu_y)^2}{2\sigma_y^2}\right) \quad (3)$$

where μ is the average value of a given class, and σ represents the covariance matrix of the class. We decided to use this classifier, as it has a good multi-class probabilistic performance, in addition to recommended when the amount of data is not large.

Majority Voting. individual region outcomes are combined into a single prediction using an election of those values. The prediction is chosen according to the most occurrent class identified in the predictions for a given subject.

3.5 Computational Aspects

Our implementation was entirely developed in Python 3.8 using the Spyder IDE, in macOS High Sierra version 10.13.6. Our method was implemented using the following tools and techniques:

1. *Data Acquisition.* the data were stored into folders labeled *id_class*, *id* is the subjects id and varies between 1 and 34, and class is labeled *M* for TS subjects and *H* otherwise;

2. *Volume Segmentation.* bash files were produced to apply the Freesurfer tool using the command *recon − all* automatically. Then, a code was used to group the intersection between regions across the subjects, remaining only the subjects' regions;

3. *Feature Extraction.* a code was developed to extract the GLCM features using the library pyRadiomics, NumPy and Pandas;

4. *Classification and Majority Voting.* the classification was performed using a code developed in python using the Naive Bayes contained in the library scikit-learn. The majority voting was entirely developed using NumPy and Pandas.

All source codes used in the implementation, in addition to the design of the experiment and the graphic are available publicly in our Github directory [1]

4 RESULTS AND DISCUSSION

In this section, two aspects were taken into account: (1) effectiveness of our approach; (2) region analysis compared with the state-of-the-art.

Four metrics were employed to evaluate our results: (1) recall - R; (2) precision - P; (3) f-measure - F; (4) accuracy - Acc. They are calculated by combining the *true-positive* (TP), *true-negative* (TN), *false-positive* (FP), *false-negative* (FN) values. The equations are defined as follows:

$$R = \frac{TP}{TP + FP} \quad (4)$$

$$P = \frac{TP}{TP + FN} \quad (5)$$

$$F = \frac{2 * R * P}{R + P} \quad (6)$$

$$Acc = \frac{TP + TN}{TP + TN + FP + FN} \quad (7)$$

---

[1] https://github.com/muribarros/TS_Feature_Extractor.git

The NB classifies the outcome for each one of the thirty chosen brain anatomical regions, returning the values of the metrics related how predictive the region was to infer whether a subject has TS or not. Figure 7 shows the accuracy value of thirty anatomical regions, where some nomenclature should be defined as: Corpus Callosum (CC) and Cerebrospinal Fluid (CSF). Among them, sixteen regions ranked greater than 60% of accuracy.

The most predictive region, according to the results, was the right-side accumbens (Acc:68%); this region is considered as the neural interface between action and motivation located in the basal ganglia, and it is the main component of the ventral striatum and plays an essential role in the understanding of neuroanatomical aspects of TS (Brito, 1997; Volman et al., 2013).

There is a significant influence on the right hemisphere of the brain, which is related to creative thinking when compared to the left hemisphere, related to analytical thinking. Studies in the literature address the importance of the amygdala, ranked in 9th position in TS due to belonging to the limbic system and how it is a reliable region to identify a subject who has TS (Neuner et al., 2010).

According to Caminiti (Caminiti et al., 2009), the *Corpus Callosum* (CC) is the primary means of communication between the brain's hemispheres, connecting cortical regions. The region has the following connections, depending on the analyzed area: (1) CC anterior, connecting with Parietal areas; (2) CC central, connecting with the motor, sensory and visual areas; (3) CC posterior, connecting with the prefrontal cortex. CC Central, CC mid-posterior, and CC posterior have achieved the second, third, and fourth positions in the top 5 most predictive brain regions for TS. This outcome goes hand in hand with the importancestate-of-the-art, which declares the importance of CC related to motor tics (Muellner et al., 2015; Steeves et al., 2010; Greene et al., 2016a).

Although analyzing single region is crucial to infer its variation in subject with TS, it is vital to assume a better prediction by combining the most predictive regions outcome. Table 2 and 3 defines the effectiveness of the top 5 most predictive regions. In addition, it is also shown that combining the anatomical regions' outcomes is more predictive to identify TS than the outcomes analyzed separately.

In the state of the art, no works were found that use the *Naive Bayes* classification. However, there are studies such as the one by (Greene et al., 2016b) that uses the *Support Vector Machine (SVM)* classification in MR images. In addition to being competitive, both works are complementary, demonstrating

Table 2: Effectiveness of the top five brain regions to detect TS.

Anatomical Region	Acc	P	R	F
I) Right Accumbens area	68%	61%	**97%**	75%
II) CC Central	66%	64%	70%	67%
III) CC Mid Posterior	66%	66%	68%	67%
IV) CC Posterior	66%	**74%**	50%	60%
V) Right choroid plexus	64%	62%	73%	67%

Table 3: Ensembles of the top regions, were top 3 first region and top 5 first region.

Ensembles	Acc	P	R	F
Top 3 regions	73%	67%	91%	77%
Top 5 regions	78%	72%	91%	80%

views of different modalities and classification characteristics.

The table 4 below illustrates the summary of the comparison of both works.

Table 4: Paper comparison.

	(Greene et al., 2016b)	Proposed method
Modality	RMf	RMs
Nº Image	84	68
Nº Anatomical Region	264	86
Atlas anatomical regions	Average fMR scans	Freesurfer
Feature Extraction	n/a	GLCM
Classification	SVM	NB
Acc fMR	70%	n/a
Acc sMR	n/a	68%
Acc Ensemble Top 3 regions sMR	n/a	73%
Acc Ensemble Top 5 regions sMR	n/a	78%

5 SUMMARY AND CONCLUSION

In this work, we have presented an approach to identify TS based on the combination of brain segmentation, feature extraction, classification, and ensemble. Our proposed workflow has four major steps: (1) we develop an approach image acquisition, which is consisted in acquiring the sMRI and study the demographic information of the subjects; (2) we develop an approach volume segmentation, which is composed of the segmenting the brain in anatomical regions; (3)
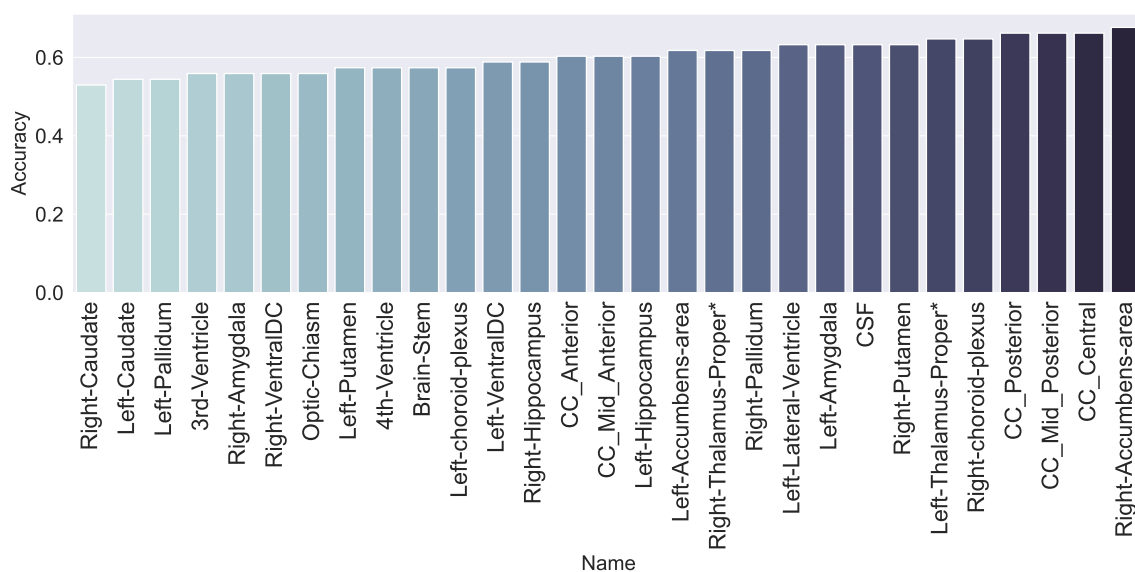
Figure 7: Best accuracies among the regions to detect TS ranked from the lowest (left) to highest (right).

we develop an approach feature extraction, responsible for identifying texture patterns in the regions via GLCM; (4) we develop an approach classification and majority voting, which classify the patients according to their regional texture patterns, combine the most significant regions into a single detection.

Tourette's syndrome is a disorder that affects motor and vocal capabilities, commonly developed in childhood. Although there is no cure, treatments are often prescribed through behavioral analysis using clinical assessment. However, this analysis may not consider imaging, which gathers reliable information about the subject's brain. Moreover, there are few works that use computational approaches thus turning into a gap to be addressed.

Our contributions in this work were: (1) proposing an approach focused on computational analysis using imaging; (2) extracting feature focusing on anatomical regions; (3) presenting a rank of the most predictive regions using Naive Bayes; (4) analyzing an ensemble to detect TS using a group of regions. Feature extraction and classification are being extensively studied in Parkinson's and Alzheimer's disease; however, those topics are not widespread in TS.

The limbic system has shown an essential part for analyzing TS since the top regions selected using our approach that reached higher accuracy belong to this system. The importance of the limbic system is also addressed in the literature but not via a computational approach. Nevertheless, the ensemble (*i.e.*, combination) of the most predictive regions' outcome has increased the detection, thus highlighting the need for detecting TS based on multiple regions outcomes. For

future work, we suggest the adoption of possible features, described as follows:

1. The use of new modalities, such as functional MRI and Positron Emission Tomography scans;

2. The use of additional anatomical regions, considering the white matter and cortical areas;

3. The use of 3D shape and texture descriptors, which may lead to a new interpretation of the regions;

4. Classification using other techniques, such as SVM, Neural Networks, and Random Forest;

ACKNOWLEDGEMENTS

REFERENCES

Brito, G. (1997). A neurobiological model for tourette syndrome centered on the nucleus accumbens. *Medical Hypotheses*, 49(2):133–142.

Caminiti, R., Ghaziri, H., Galuske, R., Hof, P. R., and Innocenti, G. M. (2009). Evolution amplified processing with temporally dispersed slow neuronal connectivity

in primates. *Proceedings of the National Academy of Sciences*, 106(46):19551–19556.

Fischl, B., Salat, D. H., Busa, E., Albert, M., Dieterich, M., Haselgrove, C., van der Kouwe, A., Killiany, R., Kennedy, D., Klaveness, S., Montillo, A., Makris, N., Rosen, B., and Dale, A. M. (2002). Whole brain segmentation: Automated labeling of neuroanatomical structures in the human brain. *Neuron*, 33(3):341–355.

Greene, D., Iii, A., Koller, J., Schlaggar, B., and Black, K. (2016a). Brain structure in pediatric tourette syndrome. *Molecular psychiatry*, 22:9.

Greene, D. J., Church, J. A., Dosenbach, N. U., Nielsen, A. N., Adeyemo, B., Nardos, B., Petersen, S. E., Black, K. J., and Schlaggar, B. L. (2016b). Multivariate pattern classification of pediatric tourette syndrome using functional connectivity mri. *Developmental Science*, 19(4):581–598.

Haralick, R. M., Shanmugam, K., et al. (1973). Textural features for image classification. *IEEE Transactions on systems, man, and cybernetics*, (6):610–621.

Hounie, A. G. (2006). *Tiques, Cacoetes, Síndrome de Tourette*, volume 1 of *1*. Artmed, The address, 1 edition.

Jafarpour, S., Sedghi, Z., and Amirani, M. C. (2012). A robust brain mri classification with glcm features. *International Journal of Computer Applications*, 37:1–5.

Kobierska, M., Sitek, M., Gocyła, K., and Janik, P. (2014). Coprolalia and copropraxia in patients with gilles de la tourette syndrome. *Neurologia i Neurochirurgia Polska*, 48(1):1–7.

Long, X., Chen, L., Jiang, C., and Zhang, L. (2017). Prediction and classification of alzheimer disease based on quantification of mri deformation. *PLoS One*, 3(12):1–19.

Muellner, J., Delmaire, C., Valabrégue, R., Schüpbach, M., Mangin, J.-F., Vidailhet, M., Lehéricy, S., Hartmann, A., and Worbe, Y. (2015). Altered structure of cortical sulci in gilles de la tourette syndrome: Further support for abnormal brain development. *Movement Disorders*, 30(5):655–661.

Muller, K. R. (2009). Prefrontal and anterior cingulate cortex abnormalities in tourette syndrome: evidence from voxel-based morphometry and magnetization transfer imaging. bmc neuroscience. *Springer Science and Business Media LLC*, pages 1–13. http://dx.doi.org/10.1186/1471-2202-10-47.

Neuner, I., Kellermann, T., Stöcker, T., Kircher, T., Habel, U., Shah, J. N., and Schneider, F. (2010). Amygdala hypersensitivity in response to emotional faces in tourette's patients. *The World Journal of Biological Psychiatry*, 11(7):858–872.

Pedrini, H. and Schwartz, W. (2008). *Análise de imagens digitais: princípios, algoritmos e aplicações*. THOMSON PIONEIRA.

Peterson, B. S., Choi, H. A., Hao, X., Amat, J. A., Zhu, H., Whiteman, R., Liu, J., Xu, D., and Bansal, R. (2007). Morphologic features of the amygdala and hippocampus in children and adults with tourette syndrome. *Archives of General Psychiatry*, 64(11):1281.

pyradiomics community (2016). Radiomic features.

Solana-Lavalle, G. and Rosas-Romero, R. (2021). Classification of ppmi mri scans with voxel-based morphometry and machine learning to assist in the diagnosis of parkinson's disease. *Computer Methods and Programs in Biomedicine*, 198:105793.

Steeves, T. D. L., Ko, J. H., Kideckel, D. M., Rusjan, P., Houle, S., Sandor, P., Lang, A. E., and Strafella, A. P. (2010). Extrastriatal dopaminergic dysfunction in tourette syndrome. *Annals of Neurology*, 67(2):170–181.

Teixeira, L. L. C., Junior, J. M. S. P., Neto, F. X. P., Targino, M. N., Palheta, A. C. P., and da Silva, F. A. (2011). Síndrome de la tourette: revisão de literatura. *Arquivos Internacionais de Otorrinolaringologia (Impresso)*.

Tinaz, S., Malone, P., Hallett, M., and Horovitz, S. G. (2015). Role of the right dorsal anterior insula in the urge to tic in tourette syndrome. *ovement Disorders, [s.l.], v. 30, n. 9*, pages 1190–1197. http://dx.doi.org/10.1002/mds.26230.

van Griethuysen, J. J., Fedorov, A., Parmar, C., Hosny, A., Aucoin, N., Narayan, V., Beets-Tan, R. G., Fillion-Robin, J.-C., Pieper, S., Aerts, H. J., and et al. (2017). Computational radiomics system to decode the radiographic phenotype. *Cancer Research*, 77(21).

Volman, S. F., Lammel, S., Margolis, E. B., Kim, Y., Richard, J. M., Roitman, M. F., and Lobo, M. K. (2013). New insights into the specificity and plasticity of reward and aversion encoding in the mesolimbic system. 33(45):17569–17576.

Zhang, W. and Gao, F. (2011). An improvement to naive bayes for text classification. *Procedia Engineering*, 15:2160–2164. CEIS 2011.